A three dimensional model of multicellular aggregate compression

Journal Name

ARTICLE TYPE

Cite this: DOI: 00.0000/xxxxxxxxxx

A three dimensional model of multicellular aggregate compression.

Chiara Giverso*[a], Salvatore Di Stefano[a], Alfio Grillo[a] and Luigi Preziosi [a]

Received Date
Accepted Date

DOI: 00.0000/xxxxxxxxxx

Multicellular aggregates are an excellent model system to explore the role of tissue biomechanics, which has been demonstrated to play a crucial role in many physiological and pathological processes. In this paper, we propose a three-dimensional mechanical model and apply it to the uniaxial compression of a multicellular aggregate in a realistic biological setting. In particular, we consider an aggregate of initially spherical shape and describe both its elastic deformations and the reorganisation of cells forming the spheroid. The latter phenomenon, understood as remodelling, is accounted for by assuming that the aggregate undergoes plastic-like distortions. The study of the compression of the spheroid, achieved by means of two parallel, compressive plates, needs the formulation of a contact problem between the living spheroid itself and the plates, and is solved with the aid of the augmented Lagrangian Method. The results of the performed numerical simulations are in qualitative agreement with the biological observations reported in the literature and can also be used to estimate quantitatively some fundamental aggregate mechanical parameters.

1 Introduction

Multicellular aggregates, and specifically multicellular spheroids (MCS), represent one of the most valid in vitro systems to study the dynamics of multicellular three-dimensional systems, being an intermediate step between monolayer growing cells and tissue culture[1,2]. In particular, living spheroids, made up of either healthy or malignant cells up to a size of 100-600 μm, are rather simple to prepare and well mimic in vivo phenomena occurring inside tissues and organs, encompassing growth, structural reorganisation, cell-cell and cell-extracellular environment interactions, response to external and endogenous stimuli, embryogenesis, malignant invasion, wound healing, and tissue engineering[1,3–8]. Furthermore, multicellular aggregates are an excellent model system to explore the role of tissue biomechanics, which has been demonstrated to play a crucial role in many physiological and pathological conditions. For instance, even though embryogenesis and morphogenesis (i.e. the complex set of events through which a living organism acquires its final shape) are under genetic control, genes by themselves do not create forms and shapes. This is achieved by physical forces, which drive structure formation in a delicate interplay of genetic, molecular and physical factors[9]. In the same way, cancer cell invasion and the formation of metastasis is controlled by genetic mutations and altered patterns of gene expression, but the physical motion of cells in the surrounding environment is determined by the mechanical properties of the cells and the extracellular environment and by their complex interactions[10–16]. Therefore, the development of three dimensional cell culture models to bridge the gap between cell-based assays and animal studies has gained the attention in the last decades, with the intent of reducing experimental uncertainties arising from monolayer cell cultures and hence the costs of subsequent in vivo drug screening processes. However, the correct interpretation of the experimental results obtained in these living multicellular settings requires the thorough understanding of the overall biophysical and mechanical properties of such systems, which emerge in a complex manner from the properties of the individual constituents (i.e. cells, extracellular matrix, liquid, vessels, etc.) forming the system and from the interplay among them, possibly mediated by subcellular molecules and organelles. This task is really challenging since cells and biological tissues are complex media, made of multiple subelements, with different me-

[a] *Department of Mathematical Sciences, Politecnico di Torino, Corso Duca degli Abruzzi, 24 – 10129 Torino (Italy), E-mail: chiara.giverso@polito.it*

chanical properties and with various biological functions[17]: each cell is bounded by the plasma membrane to form a closed object containing the nucleus and a fluid, the cytosol (made of water, soluble proteins, sugar and salt), in which numerous organelles are immersed. Each subcellular element is different from the others and mechanical properties are non-homogenously distributed inside each of them[18]. This high heterogeneity in cell composition and in subcellular properties makes mechanical and biological response difficult to be modelled even for a single cell. Furthermore, cells are able to actively interact with each other to form tissues and MCSs, containing both cells, fluids (embedded inside each cell and in the intracellular space) and possibly extracellular matrix (ECM). The rheological properties of such materials are quite uncommon and are characterized by the occurrence of many phenomena at the subcellular, cellular and macroscopic scales. The mechanical properties of the cytoskeleton, the cell membrane, the cell cytoplasm and the nucleus determine the mechanical response of an individual cell in isolation, whilst the mechanical behaviour of an ensemble of cells or a tissue is not merely the sum of each single contribution. Rather, it arises through the association and disassembling of adhesion molecules between the cells and the extracellular matrix[19,20] and through articulate mechanisms of communications and transduction of both external and internal stimuli. In general, the elastic or elasto-plastic behaviour of a MCS results from a complex interplay between cell bulk, mainly represented by cytoskeleton and organelles, and cell surface, which involves, in particular, its actomyosin cortex[21]. On the other hand, viscous effects are mainly due to the presence of the liquid. In particular, the ability of an aggregate to behave as an elasto-plastic material or as a viscous fluid depending on the experimental conditions, is related to the cell adhesion properties, to the type of interactions among the cells and to the contraction of the cell cortex. All these phenomena can lead, in general, to the presence of stress thresholds (which can be viewed as "energy barriers"[21]) that have to be overcome for the activation of the aggregate's dynanics to occur[21].

This variety of behaviours has le to the definition of many different mathematical models of multicellular aggregates and living tissues, each of them focusing on different biological aspects at different time and space scales (see Table 1 for a non-exhaustive review of previous modelling effort of quiescent multicellular aggregates and the works of Gonzalez-Rodriguez et al.[22] and Stirbat et al.[23] and Khalifat et al.[24] for a more comprehensive review of rheological properties of multicellular aggregates). Inspired by cell sorting experiments on embryonic aggregates, in most cases, tissues have been described as liquids, characterized by a viscosity and a surface tension[3,22,25]. Consequently, fluid-like constitutive equations have been advocated to model the mechanical response of growing living systems[26–28,28–34] and quiescent multicellular aggregates[22,25,35–37]. However, biological experiments[21] show that the behaviour of an aggregate can strongly deviate from the one of a liquid. Thus, this approach gives back a not completely satisfying approximation of the by far more complex behaviour of cellular aggregates, which also display solid-like properties related to the adhesive characteristics of the cells[21,38] and to the mechanical properties of the single cell in a cluster[39]. In particular, because of the occurrence of residual stresses, the stress asymptotic plateau can be sensibly higher than the one predicted by the pure surface tension in liquid models[35–37]; some aggregates (e.g. Chinese hamster ovary (CHO) cell aggregates) are not always able to fuse and round up within the time of experiments or simulations; the aggregate shape after relaxation sometimes displays a strong deviation from that of a liquid drop[21]. Thus, in some cases, cell aggregates are better described as solids with linear or nonlinear elasticity[21,40–48]. At the same time, it is not correct to consider MCSs as elastic solids, because they are composed of living material: the cells forming the aggregates duplicate and die continuously, the ECM constantly remodels because of cell reorganisation and, even in absence of growth and death, cells can rearrange their relative adhesion complexes in response to external mechanical stimuli. Moreover, living systems manifest anelastic reorganisation of the internal structure and residual stresses[41,44,49], two unique features with no analogy in liquids[50–53]. In particular, the description of such phenomena can be achieved by assuming a plastic-like behaviour of the biological structures under study[51,54]. Thus, the debate about the best mechanical modelling approach is still open and a comprehensive model of multicellular aggregates and living tissues is far from being developed. Then, a specific MCS mechanical model should be chosen depending on the phenomena we are interested in and on the time and length scale of the observation, recalling that cell aggregates behave as fluids on the timescales of cell division (mitosis) and apoptosis, which characterise growth (many hours or few days)[9,21,23,37,55,56], and as elasto-plastic solids on shorter timescales of the order of some minutes or few hours. Therefore, if we want to focus only on the description of cell compression during the time lapse of a biological experiment of the type studied in the sequel, elasto-plastic models will better describe cell behaviour, whereas the long-time fluid-like behaviour is more appropriate for capturing cell proliferation and death[55,57].

In this paper, in order to move a step towards a more realistic description of multicellular aggregate mechanical properties, we focus on the typical uniaxial compression of a living spheroid[9,25,35–37]. In this test, an initially spherical aggregate is placed on a lower compression plate, made of non-sticking (glass or steel) material, in an inner chamber filled with tissue-culture medium (maintained at 37°C by a circulating water bath through the outer chamber). The spheroid is rapidly compressed against fixed upper compression plate by a stepping motor, which is programmed to produce a deformation of a definite magni-

Table 1 Mathematical models of quiescent multicellular aggregates

Scale	Model	Constitutive behaviour	Reference
Continuous	1D adhesion energy model	liquid with surface tension	[25]
Continuous	1D adhesion energy model	viscous liquid with surface tension	[58]
Continuous	1D spring and dashpot model	visco-elastic liquid with surface tension	[35–37,59]
Continuous	1D continuous mechanical model	incompressible visco-elastic liquid	[6]
Continuous	1D continuous mechanical model	visco-elasto-plastic solid	[50,53,60,61]
Continuous	2D phase-field model	complex fluids	[62]
Continuous	dynamic network of bounded/unbounded springs	elastic	[23]
Hybrid	1D macroscopic model+ 2D Cellular Potts Model	visco-elasto-plastic material	[21]
Discrete	2D Cellular Potts Model	area and volume elastic constraint	[63]
Discrete	3D lattice model with kinetic Monte Carlo (KMC) method	surface tension constraint	[64]

tude[9,25,35–37]. Then, to perform a *stress relaxation test*, the force exerted by the aggregate on the upper plate is recorded (by measuring the apparent weight of the upper compression plate with a Cahn-Ventron electrobalance, connected to the upper compression plate[9]), while maintaining the deformation constant, until it reaches a constant stationary value. When this state is reached, the compression plates are separated and the aggregate is let free to possibly regain its initial shape (*shape recovery test*). During the release phase, the aggregate shape is continuously video recorded: it is observed that, if the compression is maintained for a very short time, the aggregate will bounce back to its initial shape, thus behaving as an elastic (or viscoelastic) solid; on the other hand, if the compression is maintained for a longer time, and if it is sufficiently high to induce the reorganization of the cellular structure, the initial configuration is no longer recovered after the compression plate is removed (at least for the times for which other phenomena, such as growth and apoptosis, do not occur). This denotes an elasto-plastic (or visco-elasto-plastic) behaviour of the living structure, which cannot be captured by the pure fluid model, based essentially on the existence of a surface tension holding together the cell aggregate[35–37].

Starting from the elasto-plastic model proposed in[50,60,65] and the elasto-visco-plastic model presented in[53,61], we here propose a three-dimensional model of multicellular aggregate compression at constant deformation, supported by three-dimensional numerical simulations of the problem in a realistic geometry in order to overcome some limitations of previous works. Specifically, in[50,60] it was proposed to apply the *theory for materials with evolving natural configurations*, introduced in[66–69], to successfully investigate cell aggregate growth and remodelling, by coupling the visco-elastic behaviors with a yield condition, generating a plastic reorganization inside the structure, when the stress becomes too high. The viscous contribution of the liquid, embedded inside the cells and filling the voids of the multicellular structure, was then introduced[53,61] in order to fit the stress-free evolutions of spheroids observed in[35–37] when the constant deformation is removed. However, in all these works[50,53,61], the representation of the whole experimental setting is highly simplified, postulating a homogeneous and constant cell density and a homogeneous deformation inside the whole body. The deformation on the normal plane to the applied force or displacement is then imposed in order to guarantee the conservation of the total aggregate volume and mass. Under these simplifying assumptions, the model was reduced to a set of two ordinary differential equations[53,61], that can be easily studied analytically. This is of course a simplification of the real phenomenon, since, even when the aggregate compression is directed only along one direction, the deformation of the living body and the cell density inside are not homogeneous and the determination of the correct shape of the system is determined by solving the mass and momentum balance inside the whole structure in the fully three dimensional setting, with proper boundary conditions. In this regard, we resort to other works[54,70–72], in which three dimensional visco-elasto-plastic models for biomechanical problems are presented. Such

works have been conceived to address totally different kind of biological tissues and biomechanical tests. Hence, they do not allow to obtain information on the mechanical behaviour of a MCS under uniaxial compression. Furthermore, those models do not tackle contact boundary conditions, which naturally occur when the aggregates boundaries come in contact with the upper and lower plates. This is a non trivial problem to solve when elasto-plasticity is involved and it causes a series of technical difficulties both in commercial softwares and in user-defined codes.

In this work we present a fully three dimensional model for cell aggregate compression and the numerical simulations considering the real biological setting. In particular the mathematical model is introduced in Section 2, then the model is numerically solved to reproduce stress relaxation experiments and shape recovery tests in Section 3. Finally, the main outcomes of this work and future improvements are discussed in Section 4.

2 Materials and Methods

Even though we do not perform the biomechanical tests on living aggregates, in order to understand the chosen modelling and numerical set-up, we here briefly report the standard protocol of the parallel-plate compression technique introduced by Steinberg and co-workers[25,35–37], which is one of the most widely used to characterize tissue properties. In this method, as already described in Section 1, an aggregate is placed inside a thermally isolated chamber filled with tissue-culture medium between two non-adhering parallel plates and compressed with a fixed deformation. A force sensor measures the evolution of the compression force, whereas the aggregate's profile is continuously video recorded.

In this section, referring to the biomechanical experiments reported in the literature, we first present the general mathematical model for a living aggregate and we then introduce the boundary conditions necessary to describe the uniaxial compression test at constant deformation. Finally we show how the proposed model can be numerically implemented.

2.1 The aggregate model

To derive the in-silico three-dimensional model of cell aggregate compression and release tests at the macroscopic scale, we refer to experimental procedures based on multicellular aggregates with radii of hundreds micrometers[25,35–37] up to some millimiters (e.g. some kind of avascular tumour spheroids). Considering a cell radius in the range of 5-10 μm, such kind of multicellular spheroids contain a number of cells of the order of thousands up to hundreds thousand of cells[1,21]. Given this high number of cells, MCS can be computationally expensive to be numerically simulated by means of discrete models and previous discrete models focused on a smaller number of cells[21,73]. Furthermore, the scale of the imposed displacements is comparable

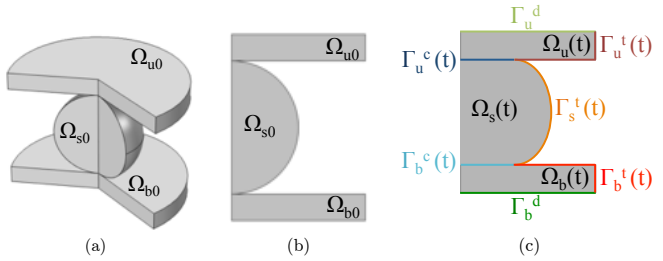

Fig. 1 Geometry of the in-silico model of cell aggregate compression. (a) Three dimensional numerical domain: Ω_{s0}, Ω_{u0} and Ω_{b0} represent the spheroid, the upper and lower plates in their reference and, in this case, initial configurations, respectively. (b) Two dimensional geometry obtained exploiting the axial symmetry of the original problem. (c) Current configurations $\Omega_s(t)$, $\Omega_u(t)$, $\Omega_b(t)$ for the spheroid, the upper and lower plates, respectively. In the picture, we sketched the Dirichlet boundary $\Gamma^d = \Gamma_u^d \cup \Gamma_b^d$, the free traction boundary $\Gamma^t(t) = \Gamma_u^t(t) \cup \Gamma_b^t(t) \cup \Gamma_s^t(t)$, and the contact boundary $\Gamma^c(t) = \Gamma_u^c(t) \cup \Gamma_b^c(t)$.

with the scale of the spheroids used in the numerical simulations and, thus, well-separated from the cell scale. Therefore, in order to obtain a general model of multicellular aggregates mechanical behaviour, continuous model could be more appropriate. Thus, we define the three regions of space at time t, $\Omega_s(t)$, $\Omega_u(t)$ and $\Omega_b(t)$ occupied, respectively, by the cellular spheroid, the upper and the bottom plates of the compressing apparatus (see Fig. 1). The boundaries of these three regions at time t are denoted with $\Gamma_s(t)$, $\Gamma_u(t)$ and $\Gamma_b(t)$. The mass and momentum balance laws in the three regions $\Omega_s(t)$, $\Omega_u(t)$ and $\Omega_b(t)$ read

$$\partial_t \rho_\alpha + \nabla \cdot (\rho_\alpha \mathbf{v}_\alpha) = 0, \qquad \text{with } \alpha = s,u,b, \quad (1)$$

$$\rho_\alpha \dot{\boldsymbol{v}}_\alpha = \rho_\alpha (\partial_t \boldsymbol{v}_\alpha + \boldsymbol{v}_\alpha \cdot \nabla \boldsymbol{v}_\alpha) = \nabla \cdot \mathbf{T}_\alpha, \qquad \text{with } \alpha = s,u,b, \quad (2)$$

where ρ_α is the mass density, $\mathbf{v}_\alpha$ is the velocity and $\mathbf{T}_\alpha$ is the Cauchy stress tensor of the material in the α-domain. We remark that, in the present setting, where a deformation is rapidly imposed to the MCS, inertial effects are not negligible. To close the equation of motion (2), together with the balance of mass (1), we need to prescribe proper constitutive equations that account for the behavior of the materials in each domain.

Mechanical response of living aggregates. As stated in Section 1, the description of the mechanical response of living systems is still an open problem. In this work, we decided to focus on the occurrence of plastic behaviours at the macroscopic scale, neglecting cell growth, viscous effects (due to the presence of the liquid encapsulated inside the structure) and other phenomena related to possible cellular heterogeneity and to mechanotransduction (i.e., the ability of cells to transform mechanical external stresses into biochemical signals and vice versa)[74]. Even in this simplified setting, living media, when subjected to external loads,

undergo an internal reorganization due to the rupture and formation of bonds among the different cells composing the aggregates[38]. This aspect poses a series of theoretical difficulties that can be adressed resorting to the theory of evolving natural configurations[41,66–68], which enables to separate the contributions related to elastic distortions from the ones related to anelastic distortions (e.g. growth and remodelling) and to model each of them individually, through a multiplicative decomposition of the deformation gradient tensor[75]. Calling Ω_{s0} and Ω_s, respectively, the reference and the actual configuration of the cellular aggregate, we introduce the smooth motion

$$\chi_s(t,\cdot) : \Omega_{s0} \longmapsto \mathbb{R}^3 , \mathbf{X} \longmapsto \mathbf{x} = \chi_s(t,\mathbf{X}) \in \Omega_s(t) \subset \mathbb{R}^3 ,$$

where $\mathbf{X}$ denotes the material coordinates associated with Ω_{s0}, whereas $\mathbf{x}$ denotes the spatial coordinates associated with Ω_s. The material gradient of the map χ_s defines the deformation gradient tensor $\mathbf{F}_s := \mathrm{Grad}\,\chi_s$.

Because of the occurence of remodeling in the living medium, the global undeformed configuration Ω_{s0} is generally not stress-free[70,75]. It is then possible to introduce the so called "natural" state Ω_{sn} of the tissue under study, understood as a collection of relaxed, or stress free, body pieces[66,75]. In this way, it is possible to decouple the deformation of the medium under study from Ω_{s0} to Ω_s into two components: the first one describes how material body pieces are distorted and relaxed towards the natural state, whereas the second one refers to the accommodating part of the deformation gradient tensor[75]. The structural changes of the MCS are modelled by means of a second-order distortion tensor, denoted with $\mathbf{F}_p$, and describing incompatible strains and material inhomogeneities triggered by cellular re-organisation[61,70,75]. On the other hand, the accommodating distortions, determining the actual configuration of the multicellular aggregate from the relaxed natural state, are represented by the second-order tensor $\mathbf{F}_n$. We remark that, although the body pieces in the natural state do not generate a configuration in the standard sense, they can be still thought of as a configuration if this is intended as a Riemannian manifold characterized by the curved metric induced by $\mathbf{F}_p$[76,77]. Hence, the multiplicative decomposition of the deformation gradient $\mathbf{F}$ reads[75,78] (see Fig. 2)

$$\mathbf{F} = \mathbf{F}_n \mathbf{F}_p .$$

We remark that neither $\mathbf{F}_p$ nor $\mathbf{F}_n$ is necessarily the gradient of a deformation. Rather, they should be regarded as primitive kinematic entities that define, together with the motion, the basic kinematic parameters that are necessary and sufficient for describing the kinematics of a remodeling living tissue[75]. In analogy with[53,54,70,75], we assume that the mechanical response from Ω_{sn} to Ω_s is hyperelastic. Of course, this is a simplification of the behaviour of a biological medium, which, in principle, would be better approximated by using a viscoelastic constitutive model.

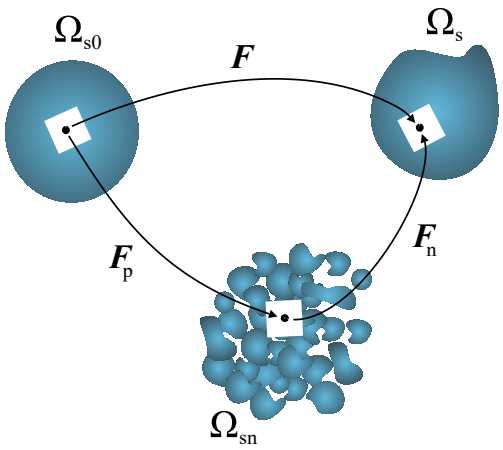

Fig. 2 Diagram of the multiplicative decomposition of the deformation gradient tensor $\mathbf{F}$ in the framework of evolving natural configurations: the reference configuration, Ω_{s0}, the current configuration, Ω_s, the natural state Ω_{sn}.

Nevertheless, since in the case of not growing living media, the characteristic times of the rate dependent response of the material are much less than the characteristic times of remodelling and of mechanical loading (expect for the loading and unloading phases)[18,79,80], the material can be thought of as hyperelastic, without introducing a significant error. The variations of volume due to the elastic and the anelastic distortions are denoted by $J_n := \det(\mathbf{F}_n)$ and $J_p := \det(\mathbf{F}_p)$, respectively, and the multiplicative decomposition of $\mathbf{F}$ implies $J := \det(\mathbf{F}) = J_n J_p$. Then, we will assume $\mathbf{F}_p$ to be isochoric, so that $J_p = 1$ and $J = J_n$

To close the description of the living aggregate behaviour we have to define the strain energy density of the system per unit volume of the natural state and prescribe a proper evolution law for $\mathbf{F}_p$. For what concerns the strain energy density we assume that the cellular aggregate can be considered to behave like an isotropic hyperelastic solid with a strain energy density of the Holmes&Mow type[81], i.e.

$$\mathscr{W}_{sn} = \alpha_0 \left[\exp(\Psi) - 1\right] , \tag{3a}$$

$$\Psi = \alpha_1 \left[I_1 - 3\right] + \alpha_2 \left[I_2 - 3\right] - \beta \log(I_3) , \tag{3b}$$

where $I_1 := \mathrm{tr}(\mathbf{C}_n)$, $I_2 := \frac{1}{2}\left[(\mathrm{tr}\mathbf{C}_n)^2 - \mathrm{tr}(\mathbf{C}_n^2)\right]$ and $I_3 := \det(\mathbf{C}_n)$ represent the three orthogonal invariants of the elastic right Cauchy–Green deformation tensor $\mathbf{C}_n = \mathbf{F}_n^T \mathbf{F}_n$, whereas $\alpha_0, \alpha_1, \alpha_2, \beta$ are the coefficients related to material properties and are related to the mechanical parameters of the tissue, the shear modulus μ and the Poisson's ratio ν, by

$$\alpha_0 = \frac{\mu(1-\nu)}{2\beta(1-2\nu)} , \quad \alpha_1 = \beta\frac{1-3\nu}{1-\nu} , \quad \alpha_2 = \beta\frac{\nu}{1-\nu} , \quad \beta = \alpha_1 + 2\alpha_2 . \tag{4}$$

Then, the Cauchy stress tensor reads

$$\mathbf{T}_\mathrm{s} \quad = \quad J_\mathrm{n}^{-1}\mathbf{F}_\mathrm{n}\left(2\frac{\partial \mathscr{W}_\mathrm{sn}}{\partial \mathbf{C}_\mathrm{n}}\right)\mathbf{F}_\mathrm{n}^{T}. \tag{5}$$

We remark that the strain energy function (3) implies a compressible multicellular aggregate. Indeed, even though, to our knowledge, quantitative measurements are not available in the literature[82], during compression, single cells inside the aggregate can highly change their volume, thanks to an exchange of liquid through the cellular membrane and even through compaction of the nuclear material[83]. Then, when we deal with incompressible media, we need to partially reformulate the continuum problem at hand, by considering incompressibility as a kinematical constraint, appended to the balance of linear momentum by means of a suitable Lagrange multiplier. In general, such method or, in the same way, penalty methods, may lead to numerical issues[84]. Thus, we preferred to consider a compressible spheroid, with a strain energy density largely employed for biological porous media[81].

The last equation needed to close the MCS mechanical description is the one governing the time evolution of the plastic-like distortions[53,54]. Because of the huge quantity of cross-links among the cells and of the low amount of extracellular matrix embedded in cellular aggregates[22], the mechanical properties of cellular aggregates results to be isotropic. In light of these considerations, the structural reorganisation of cellular spheroids relies on an isotropic description and its evolution law can be conveniently written as a time differential equation in the tensor field $\mathbf{B}_\mathrm{p} = \mathbf{F}_\mathrm{p}^{-1}\mathbf{F}_\mathrm{p}^{-T}$, which is the inverse of the right Cauchy-Green tensor $\mathbf{C}_\mathrm{p} = \mathbf{F}_\mathrm{p}^{T}\mathbf{F}_\mathrm{p}$, associated with the plastic-like distortions (see[85,86] for a review on this topic). In this context, the evolution law representing plastic-like behaviour of cellular aggregates, previously proposed by Preziosi et al.[60] and Giverso and Preziosi[61] can be recast in the form[70,87]

$$\dot{\mathbf{B}}_\mathrm{p} = -\frac{2}{\lambda_\mathrm{p}}\left[1-\frac{\tau_\mathrm{y}}{f(\mathbf{T}_\mathrm{s}')}\right]_{+}\mathbf{B}_\mathrm{p}\mathbf{M}_\mathrm{s}' \tag{6}$$

where $[\cdot]_+$ denotes the positive part of its argument, λ_p is a material parameter related to the reorganization time due to remodelling, τ_y is the yield stress of the aggregate, $f(\mathbf{T}_\mathrm{s}')$ is a frame-invariant equivalent measure of the stress $\mathbf{T}_\mathrm{s}'$, $\mathbf{M}_\mathrm{s} = J\mathbf{F}^{T}\mathbf{T}_\mathrm{s}\mathbf{F}^{-T}$ is the Mandel stress tensor of the cell aggregate and the apex $(\cdot)'$ denotes the deviatoric part of the tensor field to which it is applied. We remark that eq. (6) assumes that remodelling manifests itself as a rate-dependent plasticity model of Perzyna-type[75], which means that remodelling occurs only when $f(\mathbf{T}_\mathrm{s}')$ exceeds the threshold stress value τ_y, and is modulated by the timescale λ_p[53,61,70,75]. This assumption captures the essential phenomena occurring inside the aggregate at the cell scale: if we consider a cluster of cells subjected to a sufficiently high stress, some of the adhesive bonds among the cells may break and eventually reform in other places. Finally, we notice that, while the left-hand-side of eq. (6) is symmetric by definition, the right-hand-side is symmetric only for isotropic media, for which the Mandel stress tensor $\mathbf{M}_\mathrm{s}$ satisfies the symmetry condition[88] $\mathbf{B}_\mathrm{p}\mathbf{M}_\mathrm{s} = (\mathbf{M}_\mathrm{s}\mathbf{B}_\mathrm{p})^{T}$, as in this case. For anisotropic materials, eq. (6) is no longer valid, and the way in which remodelling is conceived must take into account the evolution of the anisotropy[71,72]. For example, this is the case of fibre-reinforced tissues, whose macroscopic mechanical properties and remodelling are substantially influenced by the distribution of the fibres embedded in the extracellular matrix.

Mechanical response of the compressive apparatus. The upper and bottom compressive plates are made of inert material, so that no biological remodelling might occur. Furthermore, their deformation is so small that plastic distortions cannot be triggered. Therefore, in the regions Ω_u and Ω_b the introduction of virtual natural configurations is not needed and we assume that the compressive apparatus behaves as a linear elastic solid, which implies that the Cauchy stress tensor can be constitutively prescribed as

$$\mathbf{T}_\alpha = \mathbb{C}_\alpha : \boldsymbol{\varepsilon}_\alpha \quad \text{in} \quad \Omega_\alpha \text{ with } \alpha = \mathrm{u},\mathrm{b} \tag{7}$$

where $\mathbb{C}_\alpha = \mathbb{C}_\alpha(E_\alpha, \nu_\alpha)$ is the fourth-order stiffness tensor, which depends on the Young's modulus E_α and the Poisson's ratio ν_α of the plates, because of the isotropy of the plates, with $\boldsymbol{\varepsilon}_\alpha = 1/2\left[\nabla\mathbf{u}_\alpha + (\nabla\mathbf{u}_\alpha)^{T}\right]$ being the infinitesimal strain tensor, given $\mathbf{u}_\alpha$ the displacement vector field inside the plates.

2.2 Boundary conditions of the aggregate model.

In order to fulfil the definition of the aggregate model, we have to assign proper conditions at the boundaries. In general, we can divide the boundary of a body into the following different regions:

1. the Dirichlet boundary $\Gamma^\mathrm{d}(t)$, on which displacements are prescribed;
2. the traction boundary $\Gamma^\mathrm{t}(t)$, on which the surface traction $\mathbf{t} = \mathbf{T}_\mathrm{s}\mathbf{n}$ is prescribed; a special case of this condition is a free surface, when $\mathbf{t} = \mathbf{0}$ is imposed;
3. the contact boundary $\Gamma^\mathrm{c}(t)$, on which the boundaries of the two adjacent domains are in contact, moving with the same normal velocity, and with the normal component of the traction continuously transferred. For frictionless contact boundaries, only the normal force is transferred, on the other hand, when friction is accounted for, the additional friction force is calculated from the relative motion of the two bodies and the contact pressure.

In particular, to describe the uniaxial compression test of cellular aggregates, we impose a null displacement on the upper side

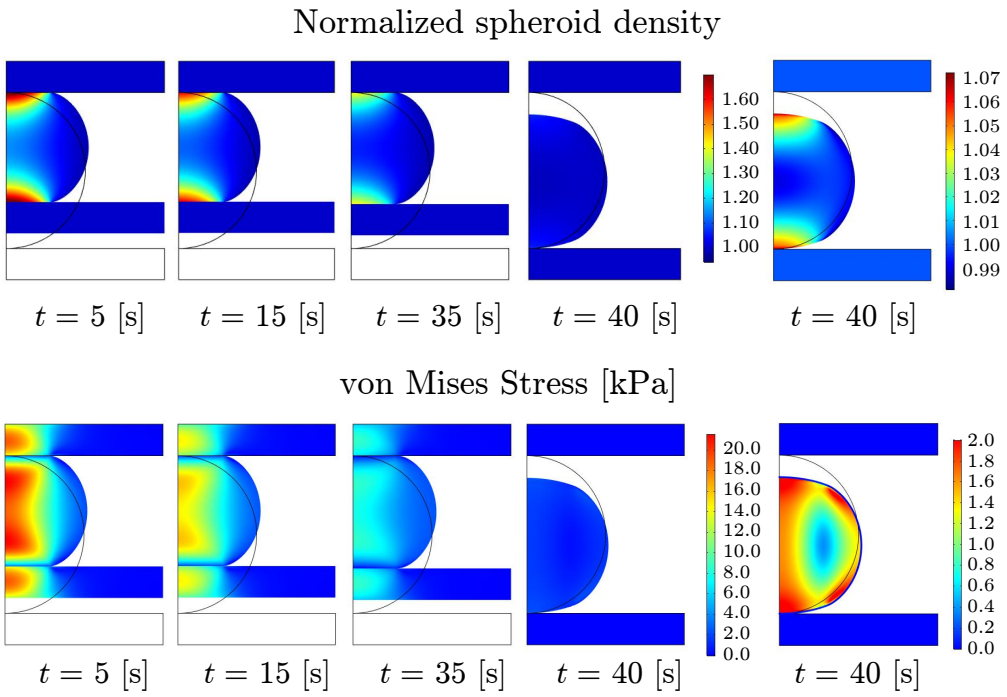

Fig. 3 Spatio-temporal evolution of the normalized spheroid density $\tilde{\rho} := \rho_s/\rho_{s0} = J^{-1}$ (top row) and von Mises stresses $T_\alpha^{mises} := \sqrt{3/2}\,||\mathbf{T}'_\alpha||$, with $\alpha = \{\mathrm{s},\mathrm{u},\mathrm{b}\}$ (bottom row) inside each domain. The loading and unloading ramp time is equal to 5 s, whereas the compression is maintained for 30 s. The simulations are obtained using $\tilde{u}_z^{max} = u_z^{max}/(2R) = 0.3$ and the set of parameters reported in Table 2.

of the upper plate $\Gamma_{\mathrm{u}}^{\mathrm{d}}(t)$ and a vertical displacement ramp $u_z(t)$ on the lower boundary of the bottom plates, $\Gamma_{\mathrm{b}}^{\mathrm{d}}(t)$, such that $\Gamma^{\mathrm{d}}(t) = \Gamma_{\mathrm{u}}^{\mathrm{d}}(t) \cup \Gamma_{\mathrm{b}}^{\mathrm{d}}(t)$ (see Fig. 1-(c)). Frictionless contact boundary conditions apply on the two contact regions between the aggregate and the upper and lower plates, $\Gamma^{\mathrm{c}}(t) = \Gamma_{\mathrm{u}}^{\mathrm{c}}(t) \cup \Gamma_{\mathrm{b}}^{\mathrm{c}}(t)$, with $\Gamma_{\mathrm{u}}^{\mathrm{c}}(t)$ and $\Gamma_{\mathrm{b}}^{\mathrm{c}}(t)$ being the contact boundary between the spheroid and the upper and bottom plate, respectively (see Fig. 1-(c)). Free surface boundary conditions are imposed on the remaining portions of the domains, $\Gamma_\alpha^{\mathrm{t}}(t)$ with $\alpha = \mathrm{s},\mathrm{u},\mathrm{b}$. We observe that, whilst the location of the boundaries $\Gamma_{\mathrm{u}}^{\mathrm{d}}$ and $\Gamma_{\mathrm{b}}^{\mathrm{d}}$ is known, the boundaries $\Gamma_{\mathrm{u}}^{\mathrm{c}}(t)$, $\Gamma_{\mathrm{b}}^{\mathrm{c}}(t)$ and $\Gamma_\alpha^{\mathrm{t}}(t)$ change in time, depending on whether the surfaces of the two bodies come in contact or detach, and that the sets $\Gamma_{\mathrm{u}}^{\mathrm{c}}(t)$ and $\Gamma_{\mathrm{b}}^{\mathrm{c}}(t)$ can possibly be empty.

Therefore, the following set of boundary conditions (BCs) describes the uniaxial compression test

$$\mathbf{u}|_{\Gamma_{\mathrm{u}}^{\mathrm{d}}} = \mathbf{0}, \tag{8}$$

$$\mathbf{u}|_{\Gamma_{\mathrm{b}}^{\mathrm{d}}} = u_z(t)\mathbf{e}_z, \tag{9}$$

$$(\mathbf{T}_\alpha \mathbf{n})|_{\Gamma_\alpha^{\mathrm{t}}} = \mathbf{0}, \qquad \text{with } \alpha = \mathrm{s},\mathrm{u},\mathrm{b}, \tag{10}$$

$$(\mathbf{v}_s \cdot \mathbf{n} - \mathbf{v}_\alpha \cdot \mathbf{n})|_{\Gamma_\alpha^{\mathrm{c}}} = 0, \qquad \text{with } \alpha = \mathrm{u},\mathrm{b}, \tag{11}$$

$$(\mathbf{n}\mathbf{T}_s\mathbf{n} - \mathbf{n}\mathbf{T}_\alpha\mathbf{n})|_{\Gamma_\alpha^{\mathrm{c}}} = 0, \qquad \text{with } \alpha = \mathrm{u},\mathrm{b}. \tag{12}$$

2.3 Finite element numerical simulations

Equations (1), (2) and (6) with the constitutive assumptions (5) and (7) and the BCs (8)-(12) were numerically solved to reproduce an unconfined uniaxial compression test of a cellular spheroid. Exploiting the symmetry of the cellular spheroid and of the compressive apparatus, the model equations can be rewritten in cylindrical coordinates and solved into the two dimensional domain of Fig. 1-(b). The top boundary of the upper plate was fixed, accordingly to the BC (8), while on the bottom boundary of the lower plate the controlled vertical displacement $u_z(t)$ was imposed. The analytical expression of $u_z(t)$ is specified later, in the context of the uniaxial compression and release test. On the remaining boundaries, stress-free boundary conditions (10) are applied when the plates and the spheroid are not in contact, while frictionless contact conditions (11)-(12) are imposed when the plates and the aggregate come into contact. We remark that the presence of contact surfaces is a source of complexity for the performed simulations. Indeed, the extent of the contact region evolves in time and is an unknown of the problem calculated from the relative displacement, which, in turn, depends on the momentum balance. Therefore, boundary conditions depend on the solution itself, so that portions of the boundary that are free with BCs of the type (10) may come in contact, thereby acquiring BCs of the type (11) and (12). In this respect, the contact

BCs (11) and (12) can be conveniently accounted for by employing the *"augmented Lagrangian method"*[89,90]. This method implements a *penalty regularization* of the standard Lagrangian multiplier method by incorporating both a Lagrange multiplier and a penalty term to solve the contact constraints and impose the conditions (11) and (12). Indeed, while in the standard formulation of the Lagrange multiplier method, the Lagrange multiplier is an unknown, in the augmented Lagrangian method, it is computed algorithmically and its initial estimation is iteratively improved, until the constraint violation is small enough (or equivalently, until the multiplier stops changing appreciably).

The Lagrangian numerical simulations have been obtained using the finite element software (FEM) COMSOL Multiphysics®(version 5.3a). The contact boundary conditions (11) and (12) are imposed by combining the routine expressly written to solve the evolution law of plastic deformations with the built-in environment for contact constraints in COMSOL Multiphysics, developed by taking inspiration of the work by Simo and Laursen[90]. We then choose a segregated approach, where the contact pressures are solved in a separate lumped step, which is the default solver when the augmented Lagrangian formulation is used. Given the numerical issues arising from the treatment of contact boundary conditions in the case of an elasto-plastic model of cellular aggregates, we have performed several tests to choose a proper mesh for solving the aggregate compression problem presented in our work. The dimension of the mesh elements at the border of the cell aggregate should be at least half the typical dimension of the elements at the upper and lower plates boundaries, to give a good resolution of the contact patch and stress state in the contact regions. In particular, computations involving a spheroid of 100 μm in radius were performed using a mesh of 7978 triangular elements in the spheroid bi-dimensional section and 380 triangular elements inside the 2D sections of each plate, for a total of 8736 elements. The number of mesh elements have then been adapted to the cases of greater spheroid radii. To verify the quality of our mesh, we have used a functionality implemented in COMSOL Multiphysics®and we have obtained a positive response. As last step, before using the mesh described so far, we have performed several refinements and solved the same benchmark tests. In doing this, we have noticed no significant changes in the results, with an increasing of the time needed to complete the simulations (i.e., few hours of computation instead of one or even more days). The choice of this kind of mesh has represented, for us, the best compromise between computational efficiency and accuracy, also in the light of running several sets of simulations.

3 Results and discussion

In this section, we apply the aggregate model presented in Section 2 to reproduce the uniaxial compression-release test of a MCS and the stress relaxation and shape recovery curves. The numerical results are discussed on the basis of available experimental data reported in the literature.

Table 2 Values of the material parameters used in the numerical simulations.

Parameter	Value in the simulations	Reference
R	$100\,\mu$m	1,3–5
λ_p	$0.001\,(\text{kPa}\cdot\text{s})^{-1}$	54
τ_y	2 kPa	87
μ	20 kPa	43,54,91,92
ν	0.2	54,91,92

3.1 Typical compression-release test

We first study the case in which the aggregate is compressed at a given deformation maintained for a certain amount of time and then released. We impose the following vertical displacement

$$u_z(t) = \begin{cases} \bar{u}_z^{max}\,\dfrac{t}{t_{ramp}}\,, & \text{for } t < t_{ramp}, \\ \bar{u}_z^{max}\,, & \text{for } t_{ramp} \le t < t_{end} - t_{ramp}, \\ -\bar{u}_z^{max}\,\dfrac{t - t_{end}}{t_{ramp}}\,, & \text{for } t_{end} - t_{ramp} \le t < t_{end}, \end{cases} \tag{13}$$

where t_{ramp} is small compared to the compression time $t_c = t_{end} - 2t_{ramp}$. Figure 3-top reports the normalized spheroid density $\tilde{\rho} := \rho_s/\rho_{s0} = J^{-1}$ in the case in which remodelling is triggered: after the sudden imposition of the deformation, the cellular density highly increases in the region close to the upper and lower plates and decreases close to the middle point of the outer boundary, where $J > 1$, as a consequence of the volumetric expansion of the spheroid along the radial direction. As the compression is maintained, the cells reorganize and redistribute inside the aggregate and the compaction of the cells inside the spheroid decreases. When the compression is released the density of cells inside the deformed aggregate continues to be inhomogeneous and different from the initial one (see last picture in the top row of Fig. 3). We remark that the total mass of the cellular spheroid is preserved during the compression and release of the cellular aggregate. Finally, we note that, the plates being slightly deformable, their normalized density is almost constant.

Looking at the distribution of the stress inside the cellular aggregate, we plot the von Mises stress $T_s^{Mises} = \sqrt{3/2}||\mathbf{T}_s'||$ inside the spheroid (see Fig. 3-bottom). In this case it is possible to observe that the maximum of the stress occurs not in the contact area but inside the spheroid, at some distance from the contact boundaries. We remark that this result recalls Hertz's theory of contact. Although this comparison may be worth further investigations, here we do not examine possible analogies with Hertz's theory because it is developed under the hypothesis of perfect elastic materials, absence of friction forces and moderate area of the contact materials. It is also possible to see that, as the compression is maintained, the stress inside the spheroid

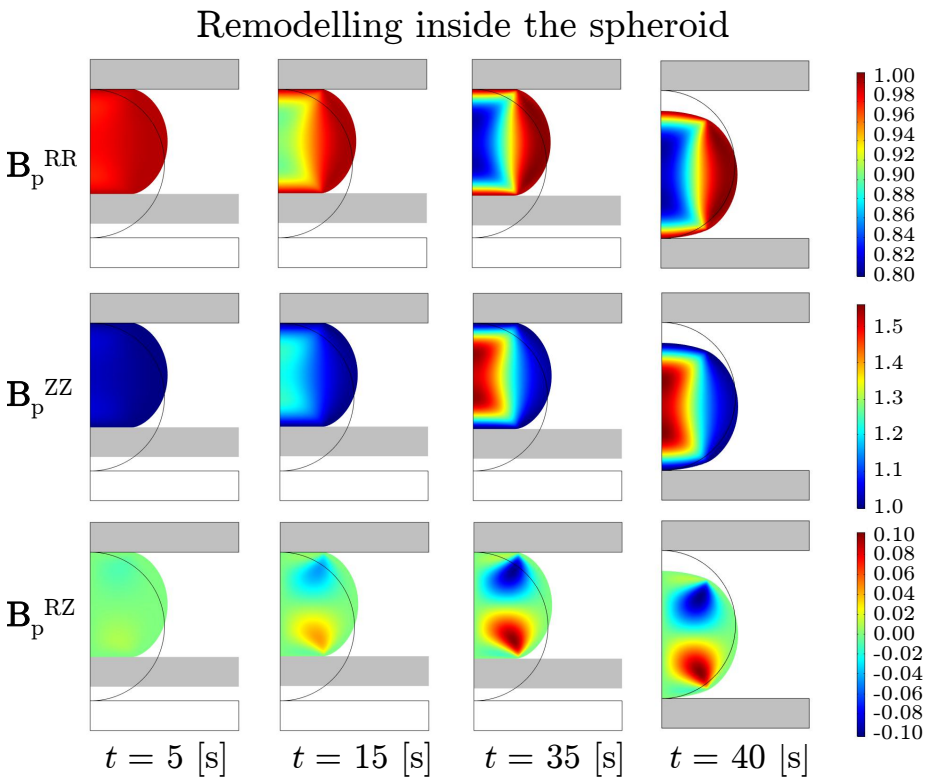

Fig. 4 Spatio-temporal evolution inside Ω_s of the components of the remodelling tensor $\mathbf{B}_\mathrm{p} = \mathbf{C}_\mathrm{p}^{-1}$ where $\mathbf{C}_\mathrm{p} = \mathbf{F}_\mathrm{p}^T\mathbf{F}_\mathrm{p}$ is the plastic Cauchy-Green deformation tensor. The parameters in the simulations are the same used for the results in Fig. 3. Notice that the in the lower and upper plate no remodelling occurs (gray regions).

decreases and, when the compression is removed, the spheroid returns stress-free at the boundary (see the blue line, reporting the normal stress, on the spheroid boundary in the last picture of Fig. 3-bottom), while residual stresses appear inside the aggregate (see last picture of Fig. 3-bottom). The amount of von Mises stress inside the multicellular structure is the chosen frame-invariant measure of the stress $f(\mathbf{T}_\mathrm{s}')$ that drives cell reorganization. Therefore, no remodelling occurs in the regions where T_s^{Mises} is below the threshold $\tau_\mathrm{y} = 2\,\mathrm{kPa}$ for plastic reorganization. In particular, if $T_\mathrm{s}^{Mises} < \tau_\mathrm{y}$ everywhere in Ω_s, the spheroid deforms elastically and no residual stresses and deformations can be observed when the imposed deformation is removed and the density of the cellular aggregate returns equal to the initial one (not shown in the figures). Furthermore, when the spheroid deforms purely elastically, no decreases in the stresses inside the multicellular structure (stress relaxation) can be observed. In fact, the decreasing of the amount of stress is due to the onset of plastic-like distortions. In this case, indeed, the stress contributes to the change of internal structure of the medium under study.

To quantify the amount of remodelling triggered by T_s^{Mises}, in Fig. 4 we report the radial, axial and shear component of the remodelling tensor $\mathbf{B}_\mathrm{p} = \mathbf{C}_\mathrm{p}^{-1}$. We observe that the radial component $B_\mathrm{p}^{\mathrm{RR}}$ is less than 1 almost everywhere in the aggregate, since, when the aggregate is compressed, remodelling in the radial direction occurs due to the expansion of the structure along the radial axis and only a small region close to the middle point of the outer boundary experiences compressive radial remodelling. The axial component B_p^{ZZ} of $\mathbf{B}_\mathrm{p}$ is bigger than 1 everywhere since remodelling occurs due to compression in the axial direction. Finally $B_\mathrm{p}^{\mathrm{RZ}}$ is a measure of the remodelling due to shear. The sign of the shear remodelling is in agreement with the convention used for shear stresses: positive shear stresses act clockwise, while negative shear stresses act counter-clockwise. The point delimiting the contact area between the spheroid and the upper plate defines the starting point of the 45° plane that identifies a change of sign in the shear remodelling. Close to the lower plate, in the region below the 45°-plane, $B_\mathrm{p}^{\mathrm{RZ}}$ is negative since shear is negative there, while in the region above the 45°-plane, $B_\mathrm{p}^{\mathrm{RZ}}$ is positive since the shear is positive there. Similar reasoning applies to the region close to the upper plate, with a change of sign due to the convention on the sign of shear stresses.

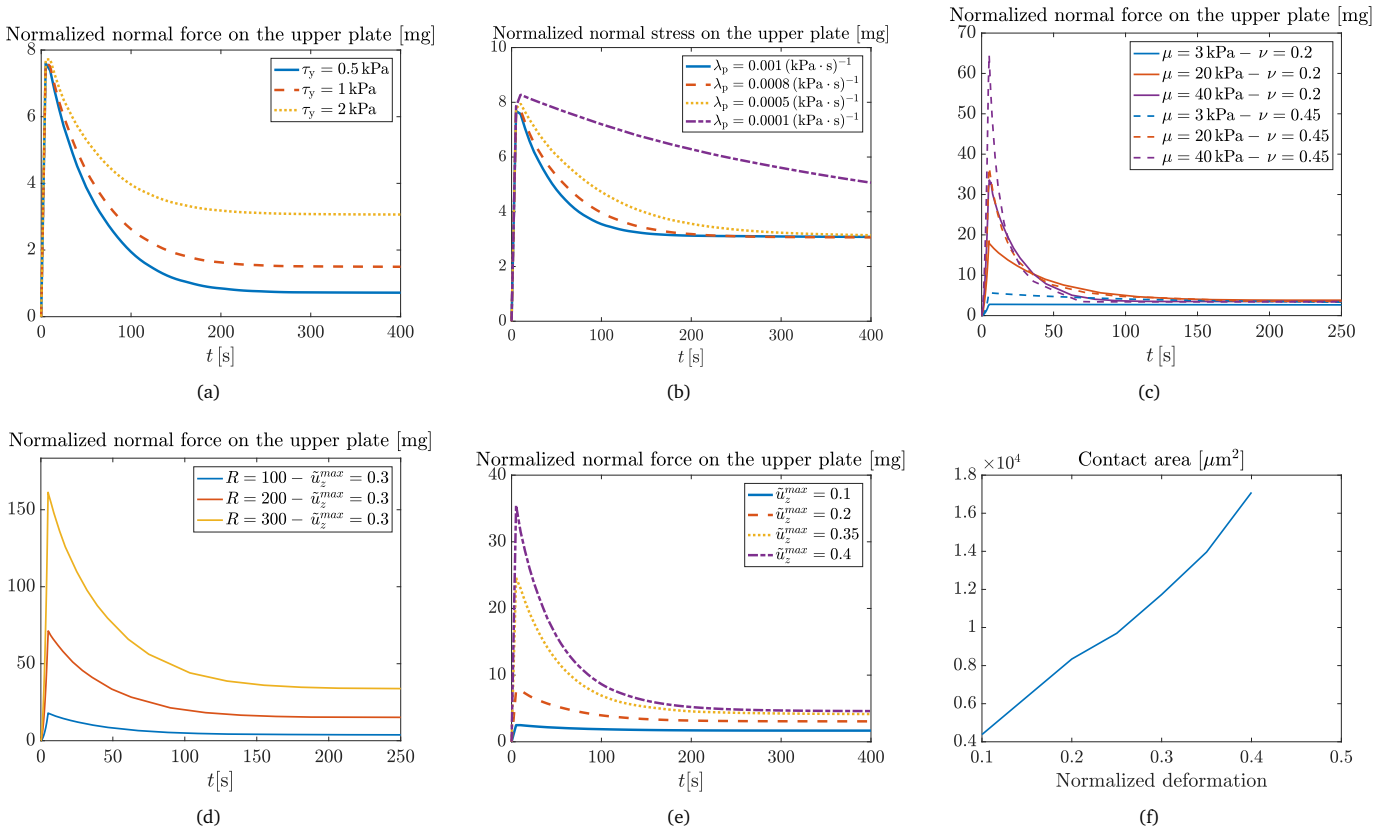

Fig. 5 Stress relaxation curves for different values of the parameters (a) τ_y, (b) λ_p, (c) μ and ν, (d) R and (e) normalized imposed deformation, i.e., $\tilde{u}_z^{max} = \bar{u}_z^{max}/(2R)$. The curves are obtained integrating the stress exerted by the aggregate over the surface of contact with the upper plate, while maintaining the compression of the aggregate at a constant deformation. (f) Contact area between the spheroid and the upper plate for different values of normalized imposed deformation, $\tilde{u}_z^{max} = \bar{u}_z^{max}/(2R)$.

3.2 Stress relaxation curves

In order to compare the predicted numerical results with the available stress relaxation curves reported in the literature[9,35–37,93], we integrate the normal stress exerted by the aggregate on the surface of contact with the upper plate to compute the total force acting on the plate, when the compression is maintained. The numerical results show that, when remodelling is triggered, the initial force transferred to the upper plate by the compressed aggregate is relaxed as the compression at constant deformation is maintained. Furthermore, the amount of relaxation of the initial force depends on the threshold stress set for the activation of plasticity, since the force exerted on the upper plate at the equilibrium depends on the value of τ_y (see Fig. 5-a). This behaviour, which is not observed when the aggregate behaves elastically, is in agreement with the results obtained in the one dimensional analysis reported by Giverso et al.[53]. The time required to relax the initial stress is related to the inverse of the parameter λ_p (see Fig. 5-b). Indeed it is possible to define the plastic reorganization time as $t_p = (\mu\lambda_p)^{-1}$, where μ is the shear modulus of the cellular aggregate. We remark that the parameter τ_y does not affect the value of the initial force exerted by the aggregate on the upper plate as shown by the maxima in Fig. 5-a, while it determines the equilibrium force on the contact areas. Conversely, λ_p does not affect the initial and the final value of force exerted on the upper plate.

In order to take into account of the variety of tissues, we have then exploited the effect of varying the cell mechanical parameters μ and ν on the MCS response. The mechanical parameters are strongly dependent on the cell type considered and a wide range of parameters can be found in the literature. Specifically, supported by biological evidences, we take the shear modulus μ varying between 3 kPa and 40 kPa[43,94] and the Poisson's ratio ν ranging between 0.2 and 0.45[43,92]. The resulting stress relaxation curves (Fig. 5-c) show that the mechanical parameters mostly affect the value of the initial stress exerted on the upper plate, with higher initial stresses for increasing value of μ. Then, for the same value of μ, the Poisson's ratio ν further magnifies the initial stress exerted on the upper plate. We also observe that, for

increasing values of the parameter μ, the plastic reorganization time decreases, accordingly to its definition, i.e., $t_p = (\mu\lambda_p)^{-1}$. On the other hand, the size parameters of the model, i.e., the radius of the spheroid R (Fig. 5-d) and the normalized imposed deformation $\bar{u}_z^{max} = \bar{u}_z^{max}/(2R)$ (Fig. 5-e), significantly influence both the initial force and the one at the stationary condition, with increasing contact forces for both increasing MCS radius (keeping $\bar{u}_{max}^z$ fix) and imposed normalized deformations (at fixed τ_y). The increase in the normalized force exerted by the aggregate on the upper plate, in the case of increasing imposed deformations, is mainly due to the increase in contact area (Fig. 5-f). Then, for very small deformations, such as for the blue curve of Fig. 5-e, the stress is slightly above the threshold value required to induce the internal reorganization of the cellular spheroid, so that the stress relaxation is less perceivable. On the other hand, as the imposed deformation increases, the stress inside the aggregate rises and the rearrangement of the cells inside the structure leads to an intense relaxation of the initial load exerted on the upper plate. Furthermore, the increase in the imposed vertical displacement leads to a higher deformation of the multicellular structure and to an almost linear increase in the contact area between the spheroid and the upper plate (Fig. 5-f).

We remark that the reported stress relaxation curves are qualitatively in agreement with the experimental curves reported in the works of Forgacs et al.[35–37], Jakab et al.[9] and Andolfi et al.[93]. Indeed, by compressing multicellular spheroids composed by either limb bud mesoderm, or heart ventricles, or livers cells taken from chicken embryos, they observed that the initial force (normalized with respect to the gravitational acceleration) exerted by the aggregate on the upper plate which is in the range 7-8 mg is relaxed to a load in the range 2.5-4 mg for a compression at constant deformation maintained for 160 s. On the other hand, in the experimental work of Jakab et al.[9] on Chinese Hamster Ovary (CHO) cells, stress relaxation is achieved on longer timescale ($\approx 400 - 1000$ s). In this work, without performing a quantitative analysis and without conducting a direct validation (which would require further biological data and details on the mechanical tests), we showed in Fig. 5 that our model is able to reproduce a sufficiently wide range of normalized stresses. We achieved that by varying the parameters of the model, so that different cellular populations can be described by varying the combination of the parameters of our model, possibly supported by other mechanical tests. Specifically, in contrast to what has been done in[35–37], where viscous effects are included, we reproduce here the typical stress relaxation curves reported in the literature by resorting solely to the reorganization of the cells inside the structure. Indeed, as anticipated in the Introduction, as long as relatively short timescales are considered, this process seems to be the fundamental mechanism occurring in the biomechanical tests addressed in this work. In fact, upon a detailed analysis of the biological experiments in which the displacement of fluorescently labeled cells is followed by confocal microscopy during aggregate compression[9], it is possible to see that tissue relaxation is driven predominantly by cell shape changes, a unique property of living systems with no analogy in liquids. Furthermore, using field emission scanning electron microscopy (FESEM) to visualize individual cells in a precompressed, compressed, and postcompressed equilibrated aggregate[9], it is possible to see that after compression a pressure gradient is set up. This is put in evidence by the fact that cells in the vicinity of the compressive plates and toward the vertical axis of symmetry of the compressed aggregate are deformed more strongly than those near the equator and side boundary, which denotes a solid-elastic behaviour of the cellular aggregate under compression, in accordance also with our simulations (before the occurrence of plasticity). Then, whilst when the aggregate is described as a viscoelastic material, any internal stress created by the initial compression is dissipated by the time the system reaches equilibrium and the remaining stresses are encapsulated only at the interface between the aggregate and the surrounding tissue culture medium[35–37], in the case of an elasto-plastic model, such as the one proposed here, residual stresses may appear inside the structure, in accordance with[41,44,49]. Therefore, even though stress relaxation curves can be reproduced only accounting for viscosity, elasto-plastic models might be more adequate to capture the biological phenomenon.

For the sake of completeness, we point out that a quantitative differences between the experimental curves[9,37,93] and the ones that can be obtained with our model are due to the possible presence of more than one relaxation time for living tissues, such as seems to be recorded in the biomechanical tests[9,37]. However, the smaller relaxation time is of the order of very few seconds[9,37] and it is probably related only to the recording of the elastic response[9] , whereas the biggest relaxation time, which is of the order of 20-40 seconds in[37,93] and 70-120 seconds in[9], reflects the global cellular rearrangement. Therefore, in the present paper, being interested in modelling anelastic behaviour in living systems, we have chosen to incorporate only the longer relaxation phenomenon which is due to the reorganization occurring inside the structure. The presence of more than one relaxation time and its origin, should be further investigated and clarified before being properly included in a MCS model.

3.3 Shape recovery curves

In this Section, we study the shape recovery behaviour of cellular aggregates after the release of a constant deformation maintained for different compression times $t_c = t_{end} - 2t_{ramp}$. As observed in the previous subsection, whilst the shape relaxation curve reported in the literature can be reproduced even without resorting to the plastic-like behaviour of the aggregate, the capability of the multicellular structure to maintain an amount of the

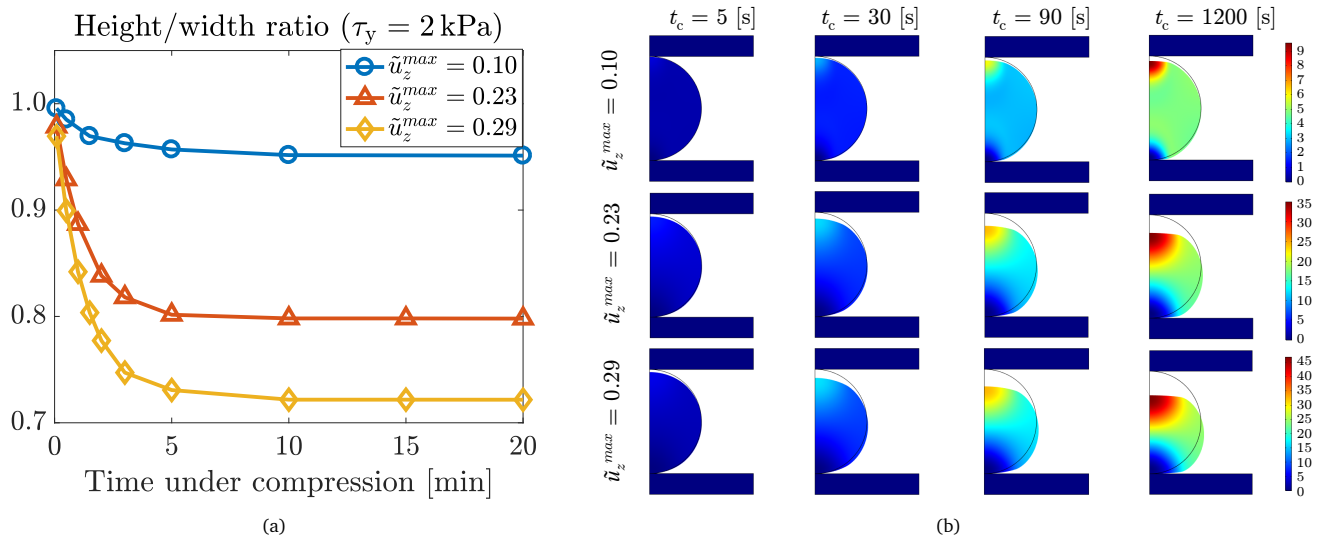

Fig. 6 (a) Height-width ratio chart for different values of imposed deformation and (b) corresponding aggregate deformed shapes. The height-width ratio is obtained dividing the height by the width of the deformed aggregate, after release of the imposed deformation (normalized with respect to the initial diameter of the spheroid, i.e., $\tilde{u}_z^{max}/(2R)$), for different values of compression time $t_c = t_{end} - 2t_{ramp}$. On the right the displacement inside the spheroid is plotted.

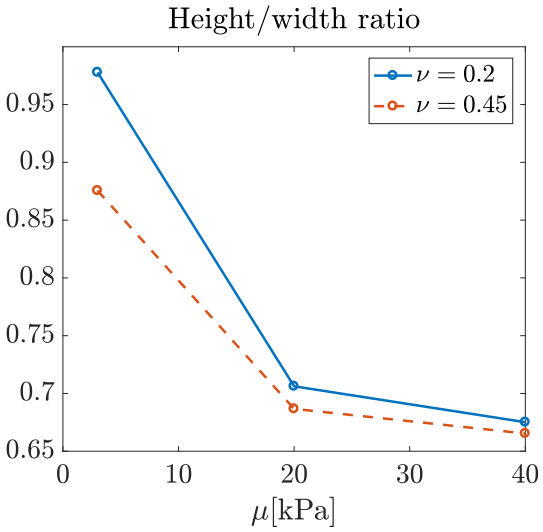

Fig. 7 Height-width ratio at the stationary state for different values of μ and ν, for an imposed deformation of $\tilde{u}_z^{max} = 0.3$.

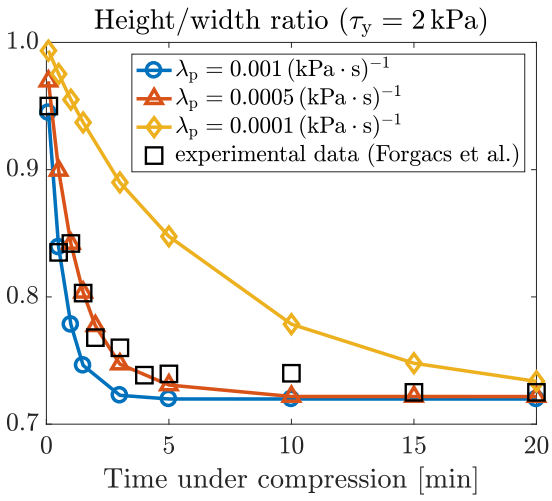

Fig. 8 Height-width ratio chart for different values of λ_p, for an imposed deformation of $\tilde{u}_z^{max} = 0.29$. The numerical results are compared with the experimental results extrapolated from the work of Forgacs et al.[37].

imposed deformation when the compression is released cannot be explained using a simple viscoelastic model. Indeed, as observed in the work of Forgacs et al.[36,37], when the compression is released, cell aggregates that were subjected to a very brief compression spring back almost to their original shapes, whereas multicellular structures compressed for a longer time do not. In particular, if the shape of the aggregates after deformation released is observed for 10-15 minutes, the MCSs maintain their deformed shape. Only incubating the aggregates for 24 hours will lead to cell spheroids rounding up again, which is probably due to the occurrence of other reorganization inside the structure and possibly cell proliferation[57]. The capability of the MCS to maintain an amount of the deformation is due to the rearrangement of the internal structure, as experimentally observed on both chick[95] and amphibian embryonic cells[96]. The rearrangement of the cell internal structure and of the bonds among the cells should be con-

verted in the model in the existence of a plastic behaviour.

Therefore, we have focused on the results obtained by means of the employment of our elasto-plastic model in the case in which the compression is maintained for different times and we report in Fig. 6-a the spheroid height over width ratio for increasing values of the cumulative time under compression, t_c, and for different values of normalized imposed deformations, $\tilde{u}_z^{max} := \bar{u}_z^{max}/(2R)$. From the reported curves it is possible to see that, in accordance with the biological evidences, if the compression is maintained for few minutes, the aggregate will bounce back to almost its initial shape, since in this case the extent of the plastic rearrangement is not consistent. On the other hand, if the compression is maintained for a longer time, the aggregate remains flattened after subsequent releases from compression, signifying the attainment of the stationary state. This is also clear from the deformed configurations reported in Fig. 6-b, where the aggregate's shape and the spatio-temporal evolution of the displacement inside the aggregate are reported for different values of cumulative time under compression and for different imposed deformations. We also show that, for the same value of normalized imposed deformation and yield stress, the total plastic deformation of the MCS is highly influenced by the mechanical parameters μ and ν (see Fig. 7), whilst it is not affected by the initial radius of the spheroid (not shown in the paper). We then compare the curves obtained from the numerical simulations for different values of λ_p with the experimental data reported in the work of Forgacs et al.[37] (see Fig. 8). It is possible to see that the best fitting for the height over width ratio curves occurs for $\lambda_p = 0.0005\,(\mathrm{kPa}\cdot\mathrm{s})^{-1}$, given an imposed deformation of 29% of the spheroid initial size. This observation is also in agreement with the experimental observation reported in the work of Jakab et al.[9], in which they observe that aggregates can be compressed up to a maximum of $\approx 30\%$ of their original diameter, in order to avoid irreversible damage to the cells and intense shape modification of the cellular structure. For the sake of completeness, we point out that the numerical height over width ratio curves have been obtained without allowing the relaxation of the MCS after each compression step, differently from what done in the experimental work of Forgacs et al.[37]. However, the difference between the numerical and the experimental protocols does not significantly affect the plastic deformation of the aggregate, since in our model we do not include viscous effects and the plastic reorganization mainly occurs during the compression phases. To confirm this theoretical expectation, we have also run a simulation in which the compression is removed at intervals (corresponding to the data points reported in Forgacs et al.[37]) and the spheroid is let free to relax for 11 s: the discrepancy between the two protocols leads to height over with ratios that differ less than 0.4% (results not shown here).

Finally, we remark that in our numerical tests, the spheroid deformation is maintained even for very long time, after the release of the imposed deformation. In order to reproduce the long-time recovery of the initial spherical shape, other factors should be included in the model, such as the presence of the external liquid and the proliferation of cells, that have not been accounted for in the present model.

4 Conclusions

Biological tissues show complex mechanical responses and their mechanical behaviour is still far from being completely understood. In this work, we aim to move a step towards this involved purpose by defining a setting to simulate the mechanical behaviour of cell aggregates when they are subjected to a uniaxial compression test. In particular, we consider an elasto-plastic model and we numerically solve it through finite element simulations by imposing contact boundary conditions to simulate the experimental set-up. With respect to previous mechanical models on aggregates[53,61], we here numerically solve the real three dimensional problem, with inhomogeneous deformation and complex shape changes. By doing this, we have provided the visualisation of a compression test on multicellular spheroids that requires the formulation of a contact problem to extract information on MCSs inelastic behaviour. We have observed, for instance, the redistribution of the spheroid's mass density in response to applied compressive loads, the reorganisation of the spheroid's internal structure, described through the inelastic variable $\boldsymbol{B}_p$, and the time evolution of the height-to-width ratio of the spheroid. From the point of view of numerical simulations, within a fully nonlinear regime, the contact boundary conditions are combined with the evolution law of plastic deformations, with the latter ones being determined by means of a routine expressly written for the works[54,70,71], and without having recourse to standard COMSOL packages. The numerical results demonstrate that the stress relaxation curves reported in the literature could be explained by assuming an elasto-plastic behaviour of the spheroids, i.e., without taking into account viscous effects, differently from previous models[35–37]. At the same time, they show that the permanent deformation observed after the application of the load/deformation can be resolved in terms of plastic deformations. The results predicted by the numerical simulations are qualitatively in agreement with the results of biological experiments and we have also proposed some quantitative comparisons in order to estimate the parameters of the model, by fitting available experimental data.

Future works will be devoted to the definition of a multiphase model of cell aggregate compression, taking into account the viscous contribution related to the presence of the culture medium liquid inside the whole structure, to account for the description of MCS non instantaneous recovery after release[35–37]. Some previous attempts to couple viscous effects with elasto-plasticity have been done, for example, in[53,61] where the viscous contribution related to the intracellular liquid is considered. However, in that case, the liquid motion is constrained to the one of the cellular

phase, whereas when an aggregate is compressed between a parallel plate apparatus, the liquid exudes from the lateral boundaries of the MCS. Conversely, when the compression is removed, the liquid will slightly fill the porous cellular structure, leading to a viscous recovery of the cell shape after compression, in agreement with the biological observation. This phenomenon can be accurately described only considering a multi-phase model, with a cellular constituent responsible of the elasto-plastic behaviour and a liquid phase carrying the viscous contribution. Furthermore, the definition of a multi-phase model will allow to investigate the mechanical contribution of the extracellular matrix that in the present model has been neglected and that can be possibly encapsulated inside living spheroids.

Another point to investigate in future works could be the role of spheroid heterogeneous shapes[97,98], that could lead to different quantitative results and to the intensification of the stresses in correspondence of bumps or, alternatively, to possible detachments in correspondence of pits in the contact region. However, heterogeneous shapes will not alter the capability of the aggregate of partially relaxing the initial stress and of giving rise to plastic deformations, as long as remodelling is triggered. In the same way, heterogeneity in the composition could lead to regions with higher/lower remodelling and to more complex MCS shapes during the compression and release processes. For moderate heterogeneities, the main results of the present work are not expected to vary significantly, although a rephrasing of the model might be necessary. Indeed, when a medium is heterogeneous, the multiplicative decomposition of the deformation gradient tensor is not sufficient, alone, to describe the structural reorganisation of the medium itself. In fact, different material responses are possible at different points of the same medium, so that the strain energy density of the spheroid must depend explicitly on the material point at which it is evaluated. Accordingly, with reference to the spheroid's natural state, one has to write $\mathscr{W}_{\mathrm{sn}}(\mathbf{C}_{\mathrm{n}},\mathbf{X})$, where the explicit dependence of $\mathscr{W}_{\mathrm{sn}}$ on $\mathbf{X}$ must be prescribed and, in principle, in a heterogeneous material it is also possible that different plastic evolution laws apply at different body points.

Future efforts will also be addressed to the definition of the active behaviour of living systems. Indeed, in spite of similarities of living tissues with inert soft materials and liquids, multicellular systems additionally display active responses that are not observed in inert soft materials[22]. In particular, the accurate description of MCS compression cannot encompass the characterization of cell active response when subjected to stresses. This response is due to mechanotransduction, which is the ability of cells to transform mechanical stresses into biochemical signals (and vice versa) in order to transfer information to and from the nucleus[18,28,74]. This ability of cells to deform and generate forces in an active manner, coupled with their extreme complexity and their non linear response to mechanical stimuli, outlines the need of a specific mathematical model to describe aggregate dynamics.

Finally, the development of specific mathematical models to describe living system responses should be supported by experimental tests. In particular, it would be interesting to perform ad hoc biological experiments in order to quantify the anelastic behaviour of such systems, determining the tissue yield stress, which physically arises from the critical force required to break intercellular bonds and induce cellular reorganization. A definitive answer to the debate of characterizing tissues as either viscoelastic fluids or visco-elasto-plastic solids could arise from measuring the frequency response of tissues to a periodic forcing[22], which is a much-needed experiment that, to our knowledge, has not been previously reported. Then, until today, models of tissue mechanics have often focused on partial descriptions of tissue behaviour that are successful in explaining specific features at a certain scale and under certain conditions. Future modelling efforts should address the general applicability of theoretical models to different tissues and various phenomena, as well as link the physics at different scales, by connecting the macroscopically measurable tissue properties to the biomolecular and intracellular mechanisms, to provide a comprehensive view of tissue mechanics[22].

In conclusion, studying tissue mechanics provides the basis to understand many physiological and pathological phenomena and to foster tissue engineering, which aims to develop new strategies of medical treatment based on artificial tissue regeneration[7,22]. Proposing a three-dimensional elasto-plastic model of living system behaviour aims at moving a step towards this ambitious goal.

Conflicts of interest

There are no conflicts to declare.

Acknowledgements

This work was partially supported by the MIUR grant "Dipartimento di Eccellenza 2018-2022", Project no. E11G18000350001 and by the INDAM grant "Progetto Giovani GNFM 2018".

Notes and references

1 R.-Z. Lin and H.-Y. Chang, *Biotechnology Journal*, 2008, **3**, 1172–1184.

2 A. Mgharbel, H. Delanoë-Ayari and J.-P. Rieu, *HFSP journal*, 2009, **3**, 213–221.

3 J. Holtfreter, *Journal of Experimental Zoology*, 1943, **94**, 261–318.

4 A. Moscona and H. Moscona, *Journal of anatomy*, 1952, **86**, 287–301.

5 W. Mueller-Klieser, *Journal of Cancer Research and Clinical Oncology*, 1987, **113**, 101–122.

6 M. Yu, A. Mahtabfar, P. Beelen, Y. Demiryurek, D. I. Shreiber, J. D. Zahn, R. A. Foty, L. Liu and H. Lin, *Biophysical Journal*, 2018, **114**, 2703–2716.

7 V. Mironov, R. P. Visconti, V. Kasyanov, G. Forgacs, C. J. Drake and R. R. Markwald, *Biomaterials*, 2009, **30**, 2164–2174.

8 L. V. Garmanchuk, E. M. Perepelitsyna, M. V. Sydorenko and L. I. Ostapchenko, *Cytology and Genetics*, 2010, **44**, 19–22.

9 K. Jakab, B. Damon, F. Marga, O. Doaga, V. Mironov, I. Kosztin, R. Markwald and G. Forgacs, *Developmental Dynamics*, 2008, **237**, 2438–2449.

10 P. Friedl and K. Wolf, *Nature Reviews Cancer*, 2003, **3**, 362–374.

11 P. Friedl, *Current Opinion in Cell Biology*, 2004, **16**, 14–23.

12 E. Sahai, *Current Opinion in Genetics & Development*, 2005, **15**, 87–96.

13 A. R. Skovoroda, A. N. Klishko, D. A. Gusakyan, Y. I. Mayevskii, V. D. Yermilova, G. A. Oranskaya and A. P. Sarvazyan, *Biophysics*, 1995, **40**, 1359–1364.

14 L. A. Taber, *ASME Appl. Mech. Rev.*, 1995, **48**, 487–545.

15 M. Lekka, P. Laidler, D. Gil, J. Lekki, Z. Stachura and A. Hrynkiewicz, *Eur. Biophys. J.*, 1999, **28**, 312–316.

16 B. S. Winters, S. R. Shepard and R. A. Foty, *International Journal of Cancer*, 2005, **114**, 371–379.

17 A. Vaziri and A. Gopinath, *Nat. Materials*, 2008, **7**, 15–23.

18 C. Verdier, J. Etienne, A. Duperray and L. Preziosi, *Comptes Rendus Physique*, 2009, **10**, 790–811.

19 A. Blumlein, N. Williams and J. J. McManus, *Scientific Reports*, 2017, **7**, 7346.

20 L. D. Muiznieks and F. W. Keeley, *Biochimica et Biophysica Acta (BBA) - Molecular Basis of Disease*, 2013, **1832**, 866–875.

21 P. Marmottant, A. Mgharbel, J. Käfer, B. Audren, J.-P. Rieu, J.-C. Vial, B. van der Sanden, A. F. M. Marée, F. Graner and H. Delanoë-Ayari, *Proceedings of the National Academy of Sciences*, 2009, **106**, 17271–17275.

22 D. Gonzalez-Rodriguez, K. Guevorkian, S. Douezan and F. Brochard-Wyart, *Science*, 2012, **338**, 910–917.

23 T. Vasilica Stirbat, S. Tlili, T. Houver, J. P. Rieu, C. Barentin and H. Delanoë-Ayari, *The European Physical Journal E*, 2013, **36**, 1–14.

24 N. Khalifat, G. Beaune, U. Nagarajan, F. M. Winnik and F. Brochard-Wyart, *Japanese Journal of Applied Physics*, 2016, **55**, 1102A8.

25 M. Steinberg, *Science*, 1963, **141**, 401–408.

26 D. Ambrosi and L. Preziosi, *Mathematical Models and Methods in Applied Sciences*, 2002, **12**, 737–754.

27 D. McElwain and G. Pettet, *Bulletin of Mathematical Biology*, 1993, **55**, 655–674.

28 C. Chen, H. Byrne and J. King, *Journal of Mathematical Biology*, 2001, **43**, 191–220.

29 K. A. Landman and C. P. Please, *Mathematical Medicine and Biology*, 2001, **18**, 131–158.

30 H. Byrne and M. Chaplain, *Mathematical Biosciences*, 1995, **130**, 151 – 181.

31 V. Cristini, J. Lowengrub and Q. Nie, *Journal of Mathematical Biology*, 2003, **46**, 191–224.

32 A. Friedman and F. Reitich, *EJ. Math. Biol.*, 1999, **38**, 262–84.

33 H. P. Greenspan, *Studies in Applied Mathematics*, 1972, **51**, 317–340.

34 C. Giverso and P. Ciarletta, *European Physical Journal E*, 2016, **39**, year.

35 R. Foty, G. Forgacs, C. Pflegerand and M. Steinberg, *Physical Review Letters*, 1994, **72**, 2298–2301.

36 R. Foty, C. Pfleger, G. Forgacs and M. Steinberg, *Development*, 1996, **122**, 1611–1620.

37 G. Forgacs, R. Foty, Y. Shafrir and M. Steinberg, *Biophysical Journal*, 1998, **74**, 2227—-2234.

38 L. Preziosi and G. Vitale, *Mathematical Models and Methods in Applied Sciences*, 2011, **21**, 1901–1932.

39 C. Giverso, A. Arduino and L. Preziosi, *Bulletin of mathematical biology*, 2018, **80**, 1017–1045.

40 M. A. J. Chaplain and B. D. Sleeman, *Journal of Mathematical Biology*, 1993, **31**, 431–473.

41 R. Skalak, S. Zargaryan, R. K. Jain, P. A. Netti and A. Hoger, *Journal of Mathematical Biology*, 1996, **34**, 889–914.

42 D. Ambrosi and F. Mollica, *Journal of Mathematical Biology*, 2004, **48**, 477–499.

43 T. Roose, P. A. Netti, L. L. Munn, Y. Boucher and R. K. Jain, *Microvascular Research*, 2003, **66**, 204–212.

44 C. Voutouri, F. Mpekris, P. Papageorgis, A. Odysseos and T. Stylianopoulos, *PLoS ONE*, 2014, **9**, e104717.

45 R. Vandiver and A. Goriely, *Journal of Biological Dynamics.*, 2009, **3**, 180–195.

46 D. Ambrosi and F. Mollica, *Journal of Mathematical Biology*, 2004, **48**, 477–499.

47 R. Araujo and D. McElwain., *European Journal of Applied Mathematics*, 2004, **15**, 365—384.

48 J. Humphrey, *Proceedings of the Royal Society of London. Series A: Mathematical, Physical and Engineering Sciences*, 2003, **459**, 3–46.

49 T. Stylianopoulos, J. D. Martin, V. P. Chauhan, S. R. Jain, B. Diop-Frimpong, N. Bardeesy, B. L. Smith, C. R. Ferrone, F. J. Hornicek, Y. Boucher, L. L. Munn and R. K. Jain, *Proceedings of the National Academy of Sciences*, 2012, **109**, 15101–15108.

50 D. Ambrosi and L. Preziosi, *Biomechanics and Modeling in Mechanobiology*, 2009, **8**, 397—-413.

51 C. Giverso, M. Scianna and A. Grillo, *Mechanics Research Communications*, 2015, **68**, 31–39.

52 C. Giverso and L. Preziosi, *International Journal of Non-Linear Mechanics*, 2019, **108**, 20–32.

53 C. Giverso and L. Preziosi, *International Journal of Non-Linear Mechanics*, 2013, **56**, 50–55.

54 P. Mascheroni, M. Carfagna, A. Grillo, D. Boso and B. Schrefler, *Mathematics and Mechanics of Solids*, 2018, **23**, 686–712.

55 J. Ranft, M. Basan, J. Elgeti, J.-F. Joanny, J. Prost and F. Jülicher, *Proceedings of the National Academy of Sciences*, 2010, **107**, 20863–20868.

56 B. Aigouy, R. Farhadifar, D. Staple, A. Sagner, J. Röper, F. Jülicher and S. Eaton, *Cell*, 2010, **142**, 773–786.

57 A. Grillo, S. Di Stefano, A. Ramírez-Torres and M. Loverre, *GAMM-Mitteilungen*, 2019, 1–30.

58 S. Douezan, K. Guevorkian, R. Naouar, S. Dufour, D. Cuvelier and F. Brochard-Wyart, *Proceedings of the National Academy of Sciences*, 2011, **108**, 7315–7320.

59 K. Guevorkian, M.-J. Colbert, M. Durth, S. Dufour and F. m. c. Brochard-Wyart, *Phys. Rev. Lett.*, 2010, **104**, 218101.

60 L. Preziosi, D. Ambrosi and C. Verdier, *Journal of Theoretical Biology*, 2010, **262**, 35–47.

61 C. Giverso and L. Preziosi, *Mathematical Medicine and Biology: A Journal of the IMA*, 2010, **29**, 181–204.

62 X. Yang, Y. Sun and Q. Wang, *Journal of Biomechanical Engineering*, 2013, **135**, year.

63 F. m. c. Graner and J. A. Glazier, *Phys. Rev. Lett.*, 1992, **69**, 2013–2016.

64 Y. Sun and Q. Wang, *Soft Matter*, 2013, **9**, 2172–2186.

65 D. Ambrosi and F. Mollica, *International Journal of Engineering Science*, 2002, **40**, 1297–1316.

66 J. D. Humphrey and K. R. Rajagopal, *Mathematical Models and Methods in Applied Sciences*, 2002, **12**, 407–430.

67 J. D. Humphrey and K. R. Rajagopal, *Biomechanics and Modeling in Mechanobiology*, 2003, **2**, 109–126.

68 E. K. Rodriguez, A. Hoger and A. D. McCulloch, *Journal of Biomechanics*, 1994, **27**, 455–467.

69 L. A. Taber and J. D. Humphrey, *Journal of Biomechanical Engineering*, 2001, **123**, 528–535.

70 A. Grillo, R. Prohl and G. Wittum, *Continuum Mechanics and Thermodynamics*, 2016, **28**, 579–601.

71 S. Di Stefano, M. Carfagna, M. Knodel, K. Hashlamoun, S. Federico and A. Grillo, *Computing and Visualization in Science*, 2019.

72 E. Crevacore, S. Di Stefano and A. Grillo, *International Journal of Non-Linear Mechanics*, 2019, **111**, 1–13.

73 G. W. Brodland, J. Yang and J. Sweny, *HFSP Journal*, 2009, **3**, 273–281.

74 M. J. Paszek, N. Zahir, K. R. Johnson, J. N. Lakins, G. I. Rozenberg, A. Gefen, C. A. Reinhart-King, S. S. Margulies, M. Dembo, D. Boettiger, D. A. Hammer and V. M. Weaver, *Cancer Cell*, 2005, **8**, 241–254.

75 M. Mićunović, *Thermomechanics of Viscoplasticity*, Springer New York, 2009.

76 S. Di Stefano, A. Ramírez-Torres, R. Penta and A. Grillo, *International Journal of Non-Linear Mechanics*, 2018, **106**, 174–187.

77 A. Goriely, *The Mathematics and Mechanics of Biological Growth*, Springer New York, 2017.

78 E. H. Lee, *Journal of Applied Mechanics*, 1969, **36**, 1–6.

79 Y. H. Chim, L. M. Mason, N. Rath, M. F. Olson, M. Tassieri and H. Yin, *Scientific Reports*, 2018, **8**, 14462.

80 S. Moreno-Flores, R. Benitez, M. dM Vivanco and J. L. Toca-Herrera, *Nanotechnology*, 2010, **21**, 445101.

81 M. Holmes and V. Mow, *Journal of Biomechanics*, 1990, **23**, 1145–1156.

82 F. Piccinini, A. Tesei, M. Zanoni and A. Bevilacqua, *BioTechniques*, 2017, **63**, 227–229.

83 M. T. Doolin, T. S. Ornstein and K. M. Stroka, *Cells*, 2019, **8**, 427.

84 J. Bonet and R. D. Wood, *Nonlinear continuum mechanics for finite element analysis*, Cambridge university press, 1997.

85 J. Simo and T. Hughes, *Computational inelasticity.*, Springer Science & Business Media, 1988.

86 J. Simo, *Computer Methods in Applied Mechanics and Engineering*, 1988, **66**, 199–219.

87 A. Grillo, R. Prohl and G. Wittum, *Mathematics and Mechanics of Solids*, 2017, **22**, 502–527.

88 G. Maugin and M. Epstein, *International Journal of Plasticity*, 1998, **14**, 109–115.

89 P. Wriggers, J. Simo and R. Taylor, *Proceedings of the NUMETA, Swansea*, 1985, **85**, year.

90 J. Simo and T. Laursen, *Computers & Structures*, 1992, **42**, 97–116.

91 P. A. Netti, D. A. Berk, M. A. Swartz, A. J. Grodzinsky and R. K. Jain, *Cancer Research*, 2000, **60**, 2497–2503.

92 T. Stylianopoulos, J. D. Martin, M. Snuderl, F. Mpekris, S. R. Jain and R. K. Jain, *Cancer Research*, 2013, **73**, 3833–3841.

93 L. Andolfi, S. L. Greco, D. Tierno, R. Chignola, M. Martinelli, E. Giolo, S. Luppi, I. Delfino, M. Zanetti, A. Battistella, G. Baldini, G. Ricci and M. Lazzarino, *Acta Biomaterialia*, 2019, **94**, 505 – 513.

94 P. A. Netti, D. A. Berk, M. A. Swartz, A. J. Grodzinsky and R. K. Jain, *Cancer Research*, 2000, **60**, 2497–2503.

95 H. M. Phillips and M. S. Steinberg, *Proceedings of the National Academy of Sciences of the United States of America*, 1969, **64**, 121–127.

96 H. Phillips, *Integrative and Comparative Biology*, 1978, **18**, 81–93.

97 M. Zanoni, F. Piccinini, C. Arienti, A. Zamagni, S. Santi, R. Polico, A. Bevilacqua and A. Tesei, *Scientific Reports*, 2016, **6**, 19103 EP –.

98 J. C. Mombach, D. Robert, F. Graner, G. Gillet, G. L. Thomas, M. Idiart and J.-P. Rieu, *Physica A: Statistical Mechanics and*

its Applications, 2005, **352**, 525 – 534.